Opto-Electronic Advances

Original Article

2019, Vol. 2, No. 4

DOI: 10.29026/oea.2019.180030

Revealing the plasmon coupling in gold nanochains directly from the near field

Quan Sun[1,2]*, Han Yu[1], Kosei Ueno[1], Shuai Zu[1], Yasutaka Matsuo[1] and Hiroaki Misawa[1]*

We studied the near-field properties of localized surface plasmon resonances in finite linear gold nanochains using photoemission electron microscopy (PEEM). The localization of the electromagnetic field in the near-field region was mapped at high spatial resolution. By tuning the excitation laser wavelength, we can obtain the near-field spectra, from which the energy splitting between longitudinal (L) and transverse (T) plasmon modes can be revealed. In particular, the L-mode red shifts and the T-mode blue shifts with increasing chain length. The red shift of the L-mode is highly dependent on the gap distance. In contrast, the T-mode almost remains constant within the range of gap distance we investigated. This energy splitting between the L-mode and the T-mode of metallic chains is in agreement with previous far-field measurements, where it was explained by dipole-dipole near-field coupling. Here, we provide direct proof of this near-field plasmon coupling in nanochains via the above-described near-field measurements using PEEM. In addition, we explore the energy transport along the gold nanochains under excitation at oblique illumination via PEEM measurements together with numerical simulations.

Keywords: surface plasmon resonance; metallic nanochains; near-field imaging; photoemission electron microscopy

Sun Q, Yu H, Ueno K, Zu S, Matsuo Y *et al*. Revealing the plasmon coupling in gold nanochains directly from the near field. *Opto-Electron Adv* **2**, 180030 (2019).

Introduction

Metallic nanoparticles exhibit localized surface plasmon resonances (LSPRs) associated with the local field enhancement (often referred to "hot spots") around the surface of the nanoparticles. The properties of the LSPR and the spatial distribution of hot spots highly depend on the composition, size, and shape of the particles as well as the surrounding medium or substrate[1–3]. For closely assembled nanoparticle arrays or aggregates, the interparticle plasmon coupling (including near-field coupling and far-field coupling) also accounts for the properties of LSPR[4–6]. In particular, the interaction of light with one dimensional (1-D) nanoparticle chains has attracted increasing attention because of the fundamental interest in plasmon coupling and the potential use of nanoparticle chains in plasmonic waveguiding and electromagnetic energy transfer beyond the optical diffraction limit[1,7–19].

Considerable research on the plasmonic properties of 1-D metallic nanoparticle chains has shown that two LSPR modes exist, namely the longitudinal mode (L-mode) and the transverse mode (T-mode), with the polarization of the excitation light parallel and perpendicular to the chain axis, respectively. The energy splitting between these two modes has been previously reported, with the energy splitting being dependent on the gap distance and the chain length (the number of particles within a chain)[1,17]. Typically, the L-mode is significantly red-shifted, and the T-mode is insensitive or slightly blue-shifted as either the chain length is increased or the gap size is reduced. Previous studies based on far-field measurements and/or numerical simulations have shown that the energy splitting between the L-mode and the T-mode is mostly due to near-field coupling[1,13,17]. The interparticle near-field coupling leads to a shift in the frequency of the L-mode plasmon resonance that is in the opposite direction to the shift of the T-mode plasmon resonance due to the change of the restoring force acting

[1]Research Institute for Electronic Science, Hokkaido University, Sapporo 001-0021, Japan; [2]College of Electronic Science and Engineering, Jilin University, Changchun 130012, China

*Correspondence: Q Sun, E-mail: quansun@es.hokudai.ac.jp; H Misawa, E-mail: misawa@es.hokudai.ac.jp

Received 27 December 2018; accepted 12 March 2019; accepted article preview online 29 March 2019

on the oscillating electrons of the particles[1]. However, direct assessment of the energy splitting between the two modes from the near field has never been performed experimentally. Moreover, near-field imaging of the 1-D metallic nanochains is highly desired to thoroughly understand its plasmonic properties. However, only a few reports have considered such near-field studies, among which, scanning near-field optical microscopy (SNOM)[8,20–23] or Cathodoluminescence (CL) imaging[24,25] was primarily employed; in these studies, the spatial resolution is typically limited to tens of nanometers. More importantly, the near-field spectral properties of the nanochain system have not been investigated yet. The recent development of nonlinear photoemission electron microscopy (PEEM) using femtosecond laser pulses as the excitation source has been demonstrated as a promising approach to investigate the plasmonic properties of surface plasmons for both the localized modes and the propagation modes[26–37]. PEEM allows direct imaging of the near field of plasmonic nanostructures with high spatial resolution and enables collection of the near-field LSPR spectra. Application of the nonlinear PEEM technique to a system of 1-D metallic nanoparticle chains would be very helpful for better understanding the near-field properties and plasmon coupling of such nanoparticle chains.

In this article, we report experimental studies on the LSPR of finite 1-D gold nanoparticle chains via PEEM using near infrared femtosecond laser pulses as the excitation source. The near-field mapping as well as the local field enhancement sites can be precisely obtained because of the high spatial resolution of our PEEM system (~8 nm). The near-field spectra are obtained by tuning the excitation wavelength. The experimental results clearly show the energy splitting between the L-mode and T-mode LSPRs and its dependence on the chain length and gap distance. These results have the same tendency as that observed from far-field measurements. This agreement proves that the plasmon coupling within the nanochains is indeed primarily due to the near-field coupling. Furthermore, we observed the signatures for energy transport along the gold nanochains from the near-field, both in experiments and in finite difference time domain (FDTD) simulations. The energy transport holds promise for applications of plasmonic waveguiding[13–16,18].

Results and discussion

Various patterns of 1-D gold nanochains were prepared using electron-beam lithography (EBL, Elionix), followed by metal sputtering and the lift-off technique. The fabrication procedure used in this study was similar to the process described in our earlier reports[38–40]. Nb-doped TiO_2 (110) substrates, which provided the conductivity necessary for the EBL process and was compatible with the PEEM measurements, were used in this study. The constituent unit of each 1-D nanochain was a gold nanoblock with the designed dimensions of 100 nm × 100 nm in the plane of the substrate surface and 36 nm in thickness. The chains were aligned along the diagonal of the nanoblocks. Figure 1(a) shows the SEM image of an array of nanochains consisting of seven nanoblocks with the gap distance of 30 nm obtained using a field-emission scanning electron microscope (JSM-6700FT, JEOL). Gold nanochains with different chain lengths or gap distances were prepared. For each fixed chain length and gap distance, the nanochains were fabricated in a 2-D array with dimensions of 150 μm × 150 μm. Two arrays with mixed nanochains were also prepared, as shown in Figs. 1(b) and 1(c), which represent SEM images of two groups of

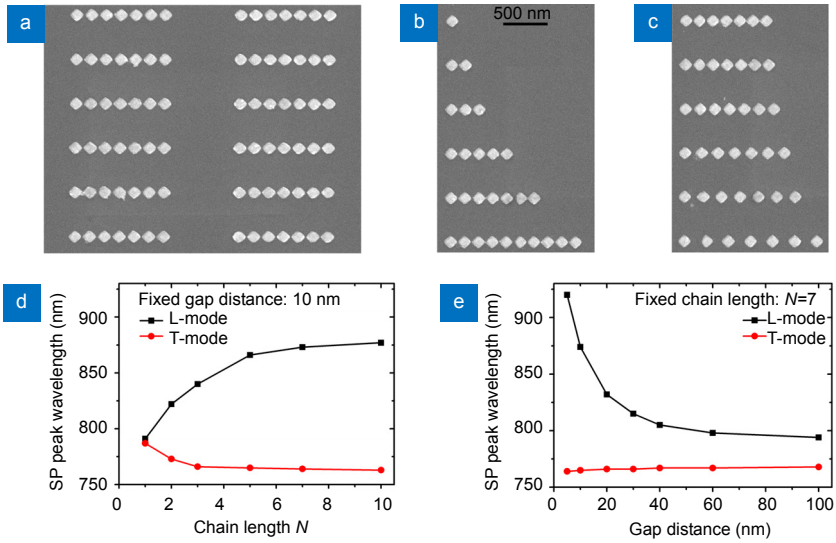

Fig. 1 | (**a**) SEM image of an array of Au nanochains on a Nb-doped TiO_2 substrate. (**b, c**) SEM images of nanochains with different chain lengths (b) and gap distances (c), respectively. (**d, e**) Plots of the L-mode and T-mode surface plasmon resonance peak wavelengths as a function of the chain length (d) and the gap size (e).

nanochains: one group with a fixed gap distance but different chain length, and another group with fixed chain length but different gap size, respectively.

The dependence of the plasmonic properties of the gold nanochains on the chain length and gap distance was assessed by measuring the optical reflection spectra of the samples using a microscopic spectrometer. The light beam from a halogen lamp was focused onto the sample by an objective lens with 40× magnification and numerical aperture *NA*=0.75. The reflected beam was collected by the same objective lens and subsequently coupled into a multichannel photodetector (PMA-11, Hamamatsu Photonics). The recorded spectra were normalized using the bare TiO_2 substrate as the reference. All the reflection spectra of the nanochains can be found in the supporting information (Fig. S1). According to these spectra, the peak wavelength of both the L-mode and the T-mode resonance as a function of the chain length and gap distance is plotted in Figs. 1(d) and 1(e), respectively. The L-mode resonance is clearly observed to undergo large red shifts whereas the T-mode resonance slightly blue shifts with the increase of the chain length. In addition, the L-mode is highly sensitive to the gap distance, whereas the T-mode is insensitive to the gap distance, that is, with the increase of the gap distance, the amount of the red-shift of the L-mode decays nearly exponentially, whereas the amount of the blue-shift of the T-mode remains unchanged or is only slightly reduced. The energy splitting between the L-mode and the T-mode increases with the increase of the chain length or with the reduction of the gap distance. These findings are consistent with the results of previous reports, where the results were interpreted due to near-field interparticle coupling via dipole-dipole interaction[1,17]. We will demonstrate whether the energy splitting still exhibits the same tendency from the near-field measurements.

The near-field measurements were performed using a photoemission electron microscope (PEEM III, Elmitec GmbH). Femtosecond laser pulses from a mode-lock Ti:Sapphire oscillator (Tsunami, Spectra-Physics) were used as the excitation source. The laser delivers 100-fs laser pulses with a central wavelength that can be tuned between 700 nm and 930 nm at a repetition rate of 77 MHz. The laser pulses were focused onto the sample surface at an angle of 74° from the surface normal by a focusing lens (focal length *f*=150 mm) with a focal spot of approximately 40 μm×150 μm. The sketch map of the light illumination is shown in Fig. 2(a). The tunable wavelength range of the laser covers the LSPR peak wavelength of the gold nanochains used in this study. Therefore, upon irradiation of the laser pulses, the LSPR of the nanochains could be efficiently excited, resulting in the plasmon-assisted nonlinear photoemission; as a result, the spatially-resolved map of photoemission could be acquired via the PEEM technique. Because of the nature of this nonlinear photoemission, the photoemission yield nonlinearly depends on the local electric field intensity; thus, the PEEM images obtained using this method could be regarded as nonlinear mapping of the near-field region of the gold nanochains. We could also perform such PEEM measurements for different excitation wavelengths, and the near-field spectra can be further obtained by integrating the photoemission yield for each wavelength.

Figures 2(c)–2(e) show the PEEM images of a typical gold nanochain with the chain length of *N*= 7 and the gap distance of 100 nm. For comparison, a mercury lamp (unpolarized cw light with maximum photon energy of 4.9 eV) was used as an additional excitation source. Upon the irradiation by the mercury lamp, uniform photoemission from the gold nanochains is observed due to the work function contrast between the gold and the TiO_2 substrate, as shown in Fig. 2(c). Upon irradiation from both the mercury lamp and p-polarized near infrared (NIR) femtosecond pulses, additional photoemission sites appeared at the corners in the axis direction (Fig. 2(d)). These additional photoemission sites appeared because the projected polarization of the incident laser in the sample surface is along the chain axis leading to the excitation of L-mode LSPR. With the excitation by the laser pulses alone, only hot spots at the corresponding corners could be observed, as shown in Fig. 2(e), resulting in the near-field mapping of the L-mode LSPR. In contrast to the previous investigations on near-field of metallic nanochains probed by SNOM, the nonlinear PEEM technique demonstrated here has better spatial resolution, and the local field enhancement sites can be intuitively

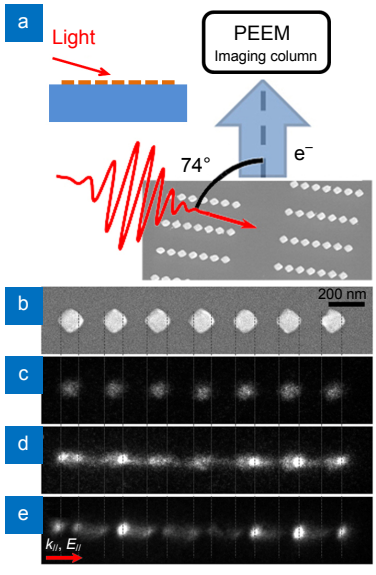

Fig. 2 | (**a**) Sketch map of the light illumination for the PEEM measurements. (**b**) SEM image of an Au nanochain with the designed gap size of 100 nm; PEEM images of the Au nanochain under different irradiation conditions: (**c**) mercury lamp, (**d**) mercury lamp and femtosecond laser pulses, and (**e**) femtosecond laser pulses. The dashed lines indicate the positions of the hot spots. The in-plane wave vector $k_{//}$ and polarization $E_{//}$ for the incident laser pulses are indicated in (e).

and precisely determined.

As mentioned above, we could measure the near-field spectra by integrating the photoemission yield over the whole field of view (*FOV*=10 μm) by varying the excitation wavelengths. We measured the near-field spectra of gold nanochains with either different chain length or different gap distance. The excitation wavelength was tuned at the step of 10 nm or 20 nm. One example of the PEEM images of the excitation nanochains under different wavelengths is shown in Fig. S2. For clarity, we only plotted three spectra for each group (L-mode and T-mode for either different chain lengths or different gap distance) in Figs. 3(a)–3(d). For a fixed gap distance of 10 nm, we found that the near-field spectrum of the L-mode (Fig. 3(a)) red shifts from 780 nm to 860 nm when the chain length increases from *N*=1 (single particle) to *N*=10, and the T-mode (Fig. 3(b)) slightly blue shifts from 800 nm to 780 nm. For fixed chain length of *N*=7, we found that the L-mode (Fig. 3(c)) dramatically red shifts from 820 nm to 920 nm when the gap distance is reduced from 100 nm to 5 nm, while the T-mode (Fig. 3(d)) remains at 780 nm with the change of the gap distance. The dependence of the peak wavelength of the LSPR probed in the near field on both the chain length and the gap distance can be presented more intuitively by the plots shown in Figs. 3(e) and 3(f). It is worth mentioning that the T-mode spectra for the fixed chain length of 7 are broadened when the gap distance is reduced. This might be due to the increased irradiative damping of the nanochains with the decrease of the gap distance. The relative inhomogeneity of the gap distance for the small gap distance could induce inhomogeneous broadening, which makes the error bar of the peak wavelength for the extreme short gap distance of 5 nm become larger (Fig. 3(f)). Nevertheless, the plots in Figs. 3(e) and 3(f) clearly show that the L-mode undergoes a large red shift when the chain length increases or the gap distance decreases, whereas the T-mode exhibits a slight blue shift when the chain length increases or remains unchanged for decreasing gap distance. They exhibit the same dependences of the LSPR peaks on the chain length and the gap distance as those observed in the far-field measurements (Figs. 1(d) and 1(e)). We argue that the plasmon coupling indeed accounts for the energy splitting that occurs in the near field. To the best of our knowledge, this observation is the first direct near-field spectral measurements of the near-field plasmon coupling of the nanochains.

The energy transport along the metallic nanochains or nanowire has been previously reported as one sequence of near-field plasmon coupling[8,12–16,18,41]. Typically, one end of the nanochain is locally excited (either by total internal reflection (TIR) of light using a prism[18] or through tight focusing onto one end[14]), and the energy propagation distance has been demonstrated to range from several hundred nanometers to several micrometers.[8,14,18]. Here, we will show that, in the case of oblique incidence, energy transport along the nanochain is also possible and can be directly observed from the near-field measurements using the PEEM technique. PEEM images of nanochains with the gap distances of 30 nm and 100 nm excited by femto-

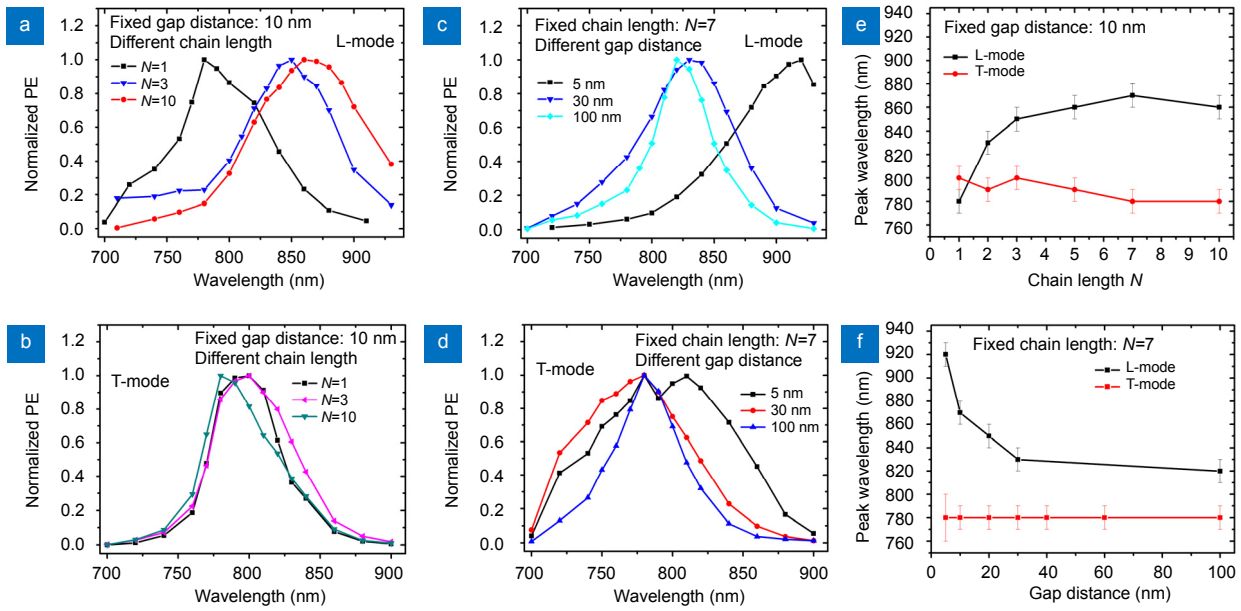

Fig. 3 | Near-field spectra of nanochains with a fixed gap distance of 10 nm but with three different chain lengths for (**a**) L-mode and (**b**) T-mode surface plasmons. (**c, d**) near-field spectra of nanochains with fixed chain length (*N*=7) but three different gap distances for L-mode and T-mode surface plasmons, respectively. (**e, f**) Summary of the dependence of both plasmon resonance peak wavelength on the chain length (e) and gap distance (f). The error bars in (e) and (f) are mainly ±10 nm, which is mainly resulted from the wavelength scan step of 10 nm. The origin of such measurement errors can account for the observed difference in peak wavelength between the L-mode and T-mode for a chain length 1 in (e).

second laser pulses at the central wavelength of 840 nm are shown in Figs. 4(a) and 4(b), respectively. The striking feature is that, in the case of the gap distance of 30 nm, the strongest hot spots are located at the distal (the right side) end of the nanochains, as shown in Fig. 4(a). Considering the laser pulses were obliquely irradiated onto the nanochains from the left side, the strong localization of the near field at the right end of the nanochains could be recognized as the energy transport along the chain. A PEEM image of one nanochain in Fig. 4(a) is plotted as a 3-D surface profile (upper figure in Fig. 4(c)), where the photoemission intensity from the distal nanoparticle is much higher than those of the other nanoparticles in the nanochain. Using the same technique as that used to obtain the data in Fig. 2, we determined that the strongest hot spot is exactly located at the outside corner of the distal nanoparticle. It is noted that the less strong photoemission spots are somehow random in Figs. 4(a) and 4(c), which is mainly resulted from the fabrication impurities. However, for the large gap distance of 100 nm, the photoemission from the last nanochain is not pronounced; instead, each nanoparticle exhibits a similar photoemission intensity, as shown in Fig. 2(e), although the intensity distribution is somehow random from one chain to another due to the small variations of the structural parameters (especially the roundedness at the corners). The results suggest that the signature of energy transport only holds for the nanochains with a relatively small gap distance.

To understand the nature of this near-field coupling and the property of energy transport, we performed finite difference time domain (FDTD, Lumerical Solutions) simulations of the near-field distribution and the surface charge distribution of the gold nanochains. In particular, the near field of two nanochains with the same chain length of N=7 but different gap distances (30 nm and 100 nm, identical to those of the chains investigated in Fig. 4) under L-mode excitation was calculated. The electric field distribution at the excitation wavelength of 840 nm on the top surface of the nanochains with the gap distance of 30 nm and 100 nm is presented in Fig. 5(a) and 5(c), respectively. It is found that, for both chains, the electric field is concentrated at the corners in the chain axis. However, some differences exist between the two near-field patterns, that is, in Fig. 5(a), the maximum local field enhancement is located at the right corner of the distal nanoparticle, and the enhancement at this site is more pronounced than at other hot spots, whereas in Fig. 5(c), the near field

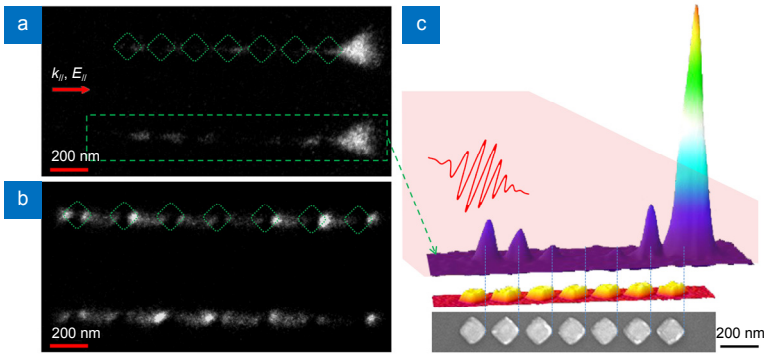

Fig. 4 | PEEM images of Au nanochains with different gap distances: (**a**) **30 nm and** (**b**) **100 nm**. The outlines of the nanochains are indicated by dotted lines. (**c**) 3-D surface plot of the photoemission intensity from one nanochain with the gap distance of 30 nm, A SEM image (bottom) and its corresponding 3-D surface plot (above the SEM image) are also presented to help indicate the location of the hotspots. The in-plane wave vector $k_{//}$ and polarization $E_{//}$ for the incident laser pulses are indicated in (a).

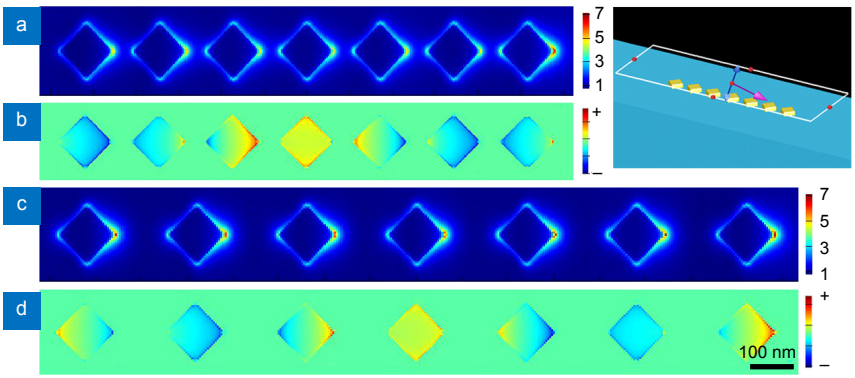

Fig. 5 | FDTD simulations of the (**a, c**) **electric field distribution and** (**b, d**) **surface charge distribution for two nanochains with different gap distances: 30 nm** (**a, b**) **and 100 nm** (**c, d**). The inset shows a sketch of the light irradiation (the blue and red arrows present the polarization and the wavelength vector of the incident light, respectively).

on each nanoparticle in the chain is almost identical. These simulation results agree well with the experimental observation shown in Fig. 4. Thus, both the experimental and simulation results suggest the energy transport along the nanochains favors those with small gap distance, for which the near-field plasmon coupling is strong.

The surface charge distribution on the nanochains was also calculated, as shown in Figs. 5(b) and 5(d). For both nanochains, the surface charges on each nanoparticle are found to oscillate in different phases, but the overall charge distribution for each of the whole chains behaves as a standing wave. We attribute such a charge distribution to the retardation effect because the phase of the light arrives at each nanoparticle is different due to the oblique illumination. As discussed in the literature[13,42], this charge distribution suggests that the plasmon resonances here can be at least partly identified as the subradiant plasmon modes because the dipole moment of each nanoparticle can be cancelled out to a certain extent. The subradiant plasmon modes reduce the radiative damping, resulting in a long propagation distance[13,43]. We argue that, in the case of oblique illumination, the efficient energy transport along the nanochains is due to both near-field plasmon coupling and the formation of subradiant-like modes induced by the retardation effect. Therefore, in the weak near-field coupling regime (large gap distance), the signature of energy transport is not obvious, despite the presence of subradiant-like plasmon modes induced by the retardation effect. In addition, in the case of normal incidence, the omnidirectional energy transport along the nanochain cannot be expected because of the symmetry (i.e., the absence of the retardation effect between adjoining nanoparticles within the nanochains). The irradiation of metallic nanochains at oblique angles should be an alternative approach for plasmonic waveguiding versus end excitation. This new approach is simpler and holds promise for providing a long propagation distance because the energy can be supplemented from each nanoparticle.

Conclusions

In conclusion, the near-field plasmonic properties of gold nanochains were investigated using PEEM with the excitation from femtosecond laser pulses. The near-field coupling in gold nanochains was directly experimentally verified from the near-field spectral measurements. The evolution of the near-field surface plasmon peak wavelengths with either the chain length or the gap distances has the same tendency as that observed from far field, providing direct proof of the near-field coupling in the nanochains. As a result of near-field coupling, the energy transport along the nanochains was also demonstrated upon oblique light irradiation. The role of the near-field coupling and subradiant plasmon modes induced by the retardation effect on the energy transport was elucidated. The results help researchers understand the nature of plasmon coupling and energy transport in metallic nanoparticle chains; such understanding will be of importance in future applications, such as plasmonic waveguiding and sensing.

References

1. Maier S A. *Plasmonics*: *Fundamentals and Applications* (Springer, New York, 2007).
2. Ueno K, Misawa H. Spectral properties and electromagnetic field enhancement effects on nano-engineered metallic nanoparticles. *Phys Chem Chem Phys* **15**, 4093–4099 (2013).
3. Kelly K L, Coronado E, Zhao L L, Schatz G C. The optical properties of metal nanoparticles: the influence of size, shape, and dielectric environment. *J Phys Chem B* **107**, 668–677 (2003).
4. Halas N J, Lal S, Chang W S, Link S, Nordlander P. Plasmons in strongly coupled metallic nanostructures. *Chem Rev* **111**, 3913–3961 (2011).
5. Wang X L, Gogol P, Cambril E, Palpant B. Near- and far-field effects on the plasmon coupling in gold nanoparticle arrays. *J Phys Chem C* **116**, 24741–24747 (2012).
6. Song H F, Sun Q, Li J, Yang F, Yang J H *et al*. Exotic mode suppression in plasmonic heterotrimer system. *J Phys Chem C* **123**, 1398–1405 (2019).
7. Barrow S J, Funston A M, Gomez D E, Davis T J, Mulvaney P. Surface plasmon resonances in strongly coupled gold nanosphere chains from monomer to hexamer. *Nano Lett* **11**, 4180–4187 (2011).
8. Maier S A, Kik P G, Atwater H A, Meltzer S, Harel E *et al*. Local detection of electromagnetic energy transport below the diffraction limit in metal nanoparticle plasmon waveguides. *Nat Mater* **2**, 229–232 (2003).
9. Wei Q H, Su K H, Durant S, Zhang X. Plasmon resonance of finite one-dimensional Au nanoparticle chains. *Nano Lett* **4**, 1067–1071 (2004).
10. Arnold M D, Blaber M G, Ford M J, Harris N. Universal scaling of local plasmons in chains of metal spheres. *Opt Express* **18**, 7528–7542 (2010).
11. De Waele R, Koenderink A F, Polman A. Tunable nanoscale localization of energy on plasmon particle arrays. *Nano Lett* **7**, 2004–2008 (2007).
12. Quinten M, Leitner A, Krenn J R, Aussenegg F R. Electromagnetic energy transport via linear chains of silver nanoparticles. *Opt Lett* **23**, 1331–1333 (1998).
13. Willingham B, Link S. Energy transport in metal nanoparticle chains via sub-radiant plasmon modes. *Opt Express* **19**, 6450–6461 (2011).
14. Solis Jr D, Willingham B, Nauert S L, Slaughter L S, Olson J *et al*. Electromagnetic energy transport in nanoparticle chains via dark plasmon modes. *Nano Lett* **12**, 1349–1353 (2012).
15. Brongersma M L, Hartman J W, Atwater H A. Electromagnetic energy transfer and switching in nanoparticle chain arrays below the diffraction limit. *Phys Rev B* **62**, R16356–R16359 (2000).
16. Maier S A, Kik P G, Atwater H A. Observation of coupled plasmon-polariton modes in Au nanoparticle chain waveguides of different lengths: estimation of waveguide loss. *Appl Phys Lett* **81**, 1714–1716 (2002).
17. Maier S A, Brongersma M L, Kik P G, Atwater H A. Observation of near-field coupling in metal nanoparticle chains using far-field polarization spectroscopy. *Phys Rev B* **65**, 193408 (2002).
18. Chen H Y, He C L, Wang C Y, Lin M H, Mitsui D *et al*. Far-field optical imaging of a linear array of coupled gold nanocubes: di-

rect visualization of dark plasmon propagating modes. *ACS Nano* **5**, 8223–8229 (2011).
19. Pocock S R, Xiao X F, Huidobro P A, Giannini V. Topological plasmonic chain with retardation and radiative effects. *ACS Photonics* **5**, 2271–2279 (2018).
20. Salerno M, Krenn J R, Hohenau A, Ditlbacher H, Schider G et al. The optical near-field of gold nanoparticle chains. Opt Commun 248, 543–549 (2005).
21. Shimada T, Imura K, Okamoto H, Kitajima M. Spatial distribution of enhanced optical fields in one-dimensional linear arrays of gold nanoparticles studied by scanning near-field optical microscopy. *Phys Chem Chem Phys* **15**, 4265–4269 (2013).
22. Kim S I, Imura K, Kim S, Okamoto H. Confined optical fields in nanovoid chain structures directly visualized by near-field optical imaging. *J Phys Chem C* **115**, 1548–1555 (2011).
23. Krenn J R, Dereux A, Weeber J C, Bourillot E, Lacroute Y *et al*. Squeezing the optical near-field zone by plasmon coupling of metallic nanoparticles. *Phys Rev Lett* **82**, 2590–2593 (1999).
24. Coenen T, Vesseur E J R, Polman A, Koenderink A F. Directional emission from plasmonic yagi-uda antennas probed by angle-resolved cathodoluminescence spectroscopy. *Nano Lett* **11**, 3779–3784 (2011).
25. Liu Z X, Jiang M L, Hu Y L, Lin F, Shen B *et al*. Scanning cathodoluminescence microscopy: applications in semiconductor and metallic nanostructures. *Opto-Electron Adv* **1**, 180007 (2018).
26. Kubo A, Onda K, Petek H, Sun Z J, Jung Y S *et al*. Femtosecond imaging of surface plasmon dynamics in a nanostructured silver film. *Nano Lett* **5**, 1123–1127 (2005).
27. Kubo A, Pontius N, Petek H. Femtosecond microscopy of surface plasmon polariton wave packet evolution at the silver/vacuum interface. *Nano Lett* **7**, 470–475 (2007).
28. Aeschlimann M, Brixner T, Fischer A, Kramer C, Melchior P *et al*. Coherent two-dimensional nanoscopy. *Science* **333**, 1723–1726 (2011).
29. Douillard L, Charra F, Korczak Z, Bachelot R, Kostcheev S *et al*. Short range plasmon resonators probed by photoemission electron microscopy. *Nano Lett* **8**, 935–940 (2008).
30. Schertz F, Schmelzeisen M, Mohammadi R, Kreiter M, Elmers H J *et al*. Near field of strongly coupled plasmons: uncovering dark modes. *Nano Lett* **12**, 1885–1890 (2012).
31. Könenkamp R, Word R C, Fitzgerald J P S, Nadarajah A, Saliba S. Controlled spatial switching and routing of surface plasmons in designed single-crystalline gold nanostructures. *Appl Phys Lett* **101**, 141114 (2012).
32. Sun Q, Ueno K, Yu H, Kubo A, Matsuo Y *et al*. Direct imaging of the near field and dynamics of surface plasmon resonance on gold nanostructures using photoemission electron microscopy. *Light*: *Sci Appl* **2**, e118 (2013).
33. Yang J H, Sun Q, Ueno K, Shi X, Oshikiri T *et al*. Manipulation of the dephasing time by strong coupling between localized and propagating surface plasmon modes. *Nat Commun* **9**, 4858 (2018).
34. Yu H, Sun Q, Ueno K, Oshikiri T, Kubo A *et al*. Exploring coupled plasmonic nanostructures in the near field by photoemission electron microscopy. *ACS Nano* **10**, 10373–10381 (2016).
35. Spektor G, Kilbane D, Mahro A K, Frank B, Ristok S *et al*. Revealing the subfemtosecond dynamics of orbital angular momentum in nanoplasmonic vortices. *Science* **355**, 1187–1191 (2017).
36. Ji B Y, Song X W, Dou Y P, Tao H Y, Gao X *et al*. Two-color multiphoton emission for comprehensive reveal of ultrafast plasmonic field distribution. *New J Phys* **20**, 073031 (2018).
37. Ji B Y, Wang Q, Song X W, Tao H Y, Dou Y P *et al*. Disclosing dark mode of femtosecond plasmon with photoemission electron microscopy. *J Phys D*: *Appl Phys* **50**, 415309 (2017).
38. Ueno K, Mizeikis V, Juodkazis S, Sasaki K, Misawa H. Optical properties of nanoengineered gold blocks. *Opt Lett* **30**, 2158–2160 (2005).
39. Ueno K, Juodkazis S, Mizeikis V, Sasaki K, Misawa H. Clusters of closely spaced gold nanoparticles as a source of two-photon photoluminescence at visible wavelengths. *Adv Mater* **20**, 26–30 (2008).
40. Wu B T, Ueno K, Yokota Y, Sun K, Zeng H P *et al*. Enhancement of a two-photon-induced reaction in solution using light-harvesting gold nanodimer structures. *J Phys Chem Lett* **3**, 1443–1447 (2012).
41. Rong K X, Gan F Y, Shi K B, Chu S S, Chen J J. Configurable integration of on-chip quantum dot lasers and subwavelength plasmonic waveguides. *Adv Mater* **30**, 1706546 (2018).
42. Wang M, Cao M, Chen X, Gu N. Subradiant plasmon modes in multilayer metal-dielectric nanoshells. *J Phys Chem C* **115**, 20920–20925 (2011).
43. Liu M Z, Lee T W, Gray S K, Guyot-Sionnest P, Pelton M. Excitation of dark plasmons in metal nanoparticles by a localized emitter. *Phys Rev Lett* **102**, 107401 (2009).

Acknowledgements

This study was supported by Grants-in-Aid for Scientific Research <KAKENHI> (Grant Nos. JP18H05205, JP17H01041, JP17H05245, and JP17H05459). We acknowledge the support from the Nanotechnology Platform (Hokkaido University) and Dynamic Alliance for Open Innovation Bridging Human, Environment and Materials (Five-Star Alliance) of MEXT. Q. Sun also acknowledges the support from the National Natural Science Foundation of China (NSFC) (No. 11527901).

Author contributions

H. Misawa supervised the project. Q. Sun and H. Yu performed the experiments. Q. Sun analysed the data and wrote the manuscript. All authors contributed to the discussion of the data and the revision of the manuscript.

Competing interests

The authors declare no competing financial interests.

Supplementary information

Supplementary information for this paper is available at https://doi.org/10.29026/oea.2019.180030